



Spatio-temporal variations of CDOM in shallow inland waters from a semi-analytical inversion of Landsat-8

Jiwei Li^a, Qian Yu^{a,*}, Yong Q. Tian^b, Brian L. Becker^b, Paul Siqueira^c, Nathan Torbick^d

^a Department of Geosciences, University of Massachusetts, Amherst, United States

^b Institute for Great Lakes Research, Department of Geography, Central Michigan University, United States

^c Department of Electrical and Computer Engineering, University of Massachusetts, Amherst, United States

^d Applied GeoSolutions, Newmarket, NH, United States

ARTICLE INFO

Keywords:

CDOM
Carbon flux
SBOP
Landsat
Carbon cycle
Optically shallow waters
Hydrology

ABSTRACT

Bottom reflectance is often the main cause of high uncertainty in Colored Dissolved Organic Matter (CDOM) estimation for optically shallow waters. This study presents a Landsat-8 based Shallow Water Bio-optical Properties (SBOP) algorithm to overcome bottom effects so as to successfully observe spatial and temporal CDOM dynamics in inland waters. We evaluated the algorithm via 58 images and a large set of field measurements collected across seasons of multiple years in the Saginaw Bay, Lake Huron. Results showed that the SBOP algorithm reduced estimation errors by as much as 4 times (RMSE = 0.17 and $R^2 = 0.87$ in the Saginaw Bay) when compared to the QAA-CDOM algorithm that did not take into account bottom reflectance. These improvements in CDOM estimation are consistent and robust across broad range CDOM absorption. Our analysis revealed: 1) the proposed remote sensing algorithm resulted in significant improvements in tracing spatial-temporal CDOM inputs from terrestrial environments to lakes, 2) CDOM distribution captured with high resolution land-viewing satellite is useful in revealing the impacts of terrestrial ecosystems on the aquatic environment, and 3) Landsat-8 OLI, with its 16 days revisit time, provides valuable time series data for studying CDOM seasonal variations at land-water interface and has the potential to reveal its relationship to adjacent terrestrial biogeography and hydrology. The study presents a shallow water algorithm for studying freshwater or coastal ecology, as well as carbon cycling science.

1. Introduction

The assessment of Colored Dissolved Organic Matter (CDOM) in lake waters help the scientific community better understand both global/regional carbon cycling and aquatic ecosystem biogeochemistry. CDOM can be used as a surrogate for terrestrially derived dissolved organic carbon (DOC) assessment (Kutser et al., 2015). The export of terrestrial DOC to lakes and oceans represents a significant carbon exchange at the land-water interface (Roulet and Moore, 2006; Tian et al., 2013). This carbon flux is a key pathway leading to widespread CO₂ supersaturation in aquatic environments (Butman et al., 2016; Jonsson et al., 2003; Raymond et al., 2013). Inland waters also play a significant role in the sequestration, transport and mineralization of terrestrially sourced organic carbon (Bastviken et al., 2011; Battin et al., 2009; Tranvik et al., 2009). In addition, soil carbon loss to rivers and lakes has an important impact on net terrestrial carbon budgets (Davidson et al., 2010). CDOM in inland waters also influences the aquatic ecosystem in

a variety of ways (Williamson et al., 1999). CDOM in inland water absorbs short wavelength incoming light, and this absorption will further affect the growth of plankton communities (Diehl, 2002; Williamson et al., 1996). Moreover, terrestrial DOC transportation to inland waters represents a very important nutrient exportation pathway from land to water (Cole et al., 2007). These terrestrial carbon inputs will ultimately impact the food webs within the lake environment (Brezonik et al., 2015; Cole et al., 2006).

Remotely sensed satellite imagery provides an efficient solution for monitoring CDOM dynamics (Keith et al., 2016). The remote sensing estimation of water biogeochemistry is based on observation of water bio-optical components, including CDOM, which influence the underwater light field (Hoge and Lyon, 1996; Yu et al., 2010), and therefore lead to changes in water leaving radiance received by the satellite sensor (Zhu et al., 2011). Previous research on inland and coastal water CDOM estimation by high-resolution satellite data often relied on empirical band ratios algorithms, in which model coefficients are specific

* Corresponding author.

E-mail address: qyu@geo.umass.edu (Q. Yu).

<https://doi.org/10.1016/j.rse.2018.09.014>

Received 19 September 2017; Received in revised form 14 September 2018; Accepted 18 September 2018

Available online 05 October 2018

0034-4257/ © 2018 Elsevier Inc. All rights reserved.

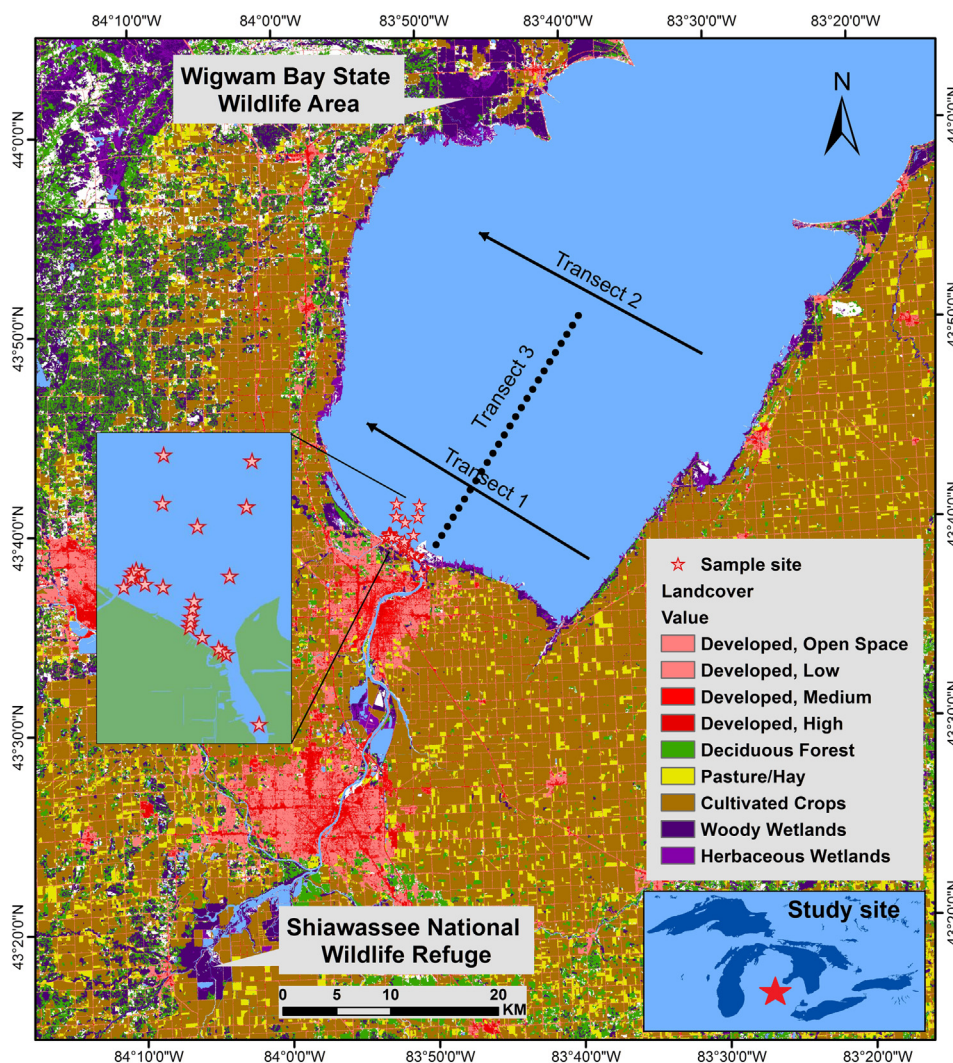


Fig. 1. The study area of Saginaw Bay, Lake Huron. The surrounding area contains varied landcover types, including wetlands, agricultural cropland, and forest. Red stars marked the filed samplings locations. (For interpretation of the references to colour in this figure legend, the reader is referred to the web version of this article.)

to site and satellite sensors. It often requires additional tuning when applied to other waterbodies (Kutser et al., 2005; Mannino et al., 2008). Sensor-independent semi-analytical algorithms based on bio-optical water radiative transfer models have been developed to improve the retrieval of water biogeochemistry, particularly chlorophyll absorption (Carder et al., 1999; Kahru and Mitchell, 2001; Le et al., 2013; Lee et al., 2002). In addition, the need to better estimate carbon amounts in coastal regions resulted in the development of several semi-analytical algorithms designed to retrieve CDOM absorption in optically deep waters (Matsuoka et al., 2013; Shanmugam, 2011; Zhu and Yu, 2013). Unfortunately, these semi-analytical CDOM algorithms are not applicable to optically shallow waters, which limit using remote sensing techniques for assessing carbon dynamics at the land-water interface. An algorithm specific to the estimation of CDOM in inland, optically shallow waters is needed.

Growing interest in inland water CDOM observation via remote sensing requires suitable satellite images with both the proper spectral wavelengths and finer spatial resolution (Brezonik et al., 2015; Palmer et al., 2015). The semi-analytical algorithms take advantage of better atmospheric correction and water properties estimation (e.g. chlorophyll) aids by an “ultra-blue” band (e.g. from 435 nm to 450 nm) to build the bio-optical model in the coastal region or temperate lake (Lee et al., 2007a; Lee et al., 2002). Consequently, the studies using semi-analytical algorithms are mainly based on the ocean-viewing satellites

(MODIS, SeaWiFS) or hyperspectral satellite sensor (EO-1 Hyperion) that record data in this wavelength range (Cuthbert and Del Giorgio, 1992; Kutser et al., 2005; Miller and McKee, 2004; O’Reilly et al., 1998;). However, these images are not applicable to studies involving smaller inland lakes and rivers because of coarse spatial resolutions (e.g., MODIS) or narrow coverage (e.g., Hyperion). Rivers, that are important pathways for transporting terrestrial CDOM, typically have a width narrower than two kilometers (Allen and Pavelsky, 2015). The spatial resolution or pixel size of most ocean-viewing sensors such as MODIS are far too coarse to observe inland waters, and much uncertainty is introduced when these images contain land-water mixed pixels (Zhu et al., 2013a). In contrast, the recently decommissioned high resolution hyperspectral sensor Hyperion had provided the spatial resolutions needed for inland waters, but its utility was very limited with respect to terrestrial CDOM estimation due to its narrow coverage and limited acquisition (Zhu and Yu, 2013). In recent years, several multispectral land-viewing satellite sensors have offered new promise for the retrieval of inland water bio-optical properties with the addition of an ultra-blue band, such as Landsat-8 and Sentinel-2 (Roy et al., 2014). In this study, we selected Landsat-8 to derive the CDOM absorption in lake waters. With its relatively high spatial resolution, Landsat 8 is able to effectively capture images of the lower reaches and plumes of rivers, thereby increasing its potential for observing inland water biogeochemistry (Pahlevan et al., 2014). Several empirical

algorithms have been applied to Landsat-8 images for observing CDOM absorption based on band-ratio methodologies in optically deep waters as mentioned above (Chen et al., 2017; Kutser et al., 2016; Olmanson et al., 2016).

This study investigates the efficacy of the SBOP algorithm (Li et al., 2017), a semi-analytical CDOM algorithm originally developed with in situ spectral data, on satellite image for shallow waters. To our knowledge, our research represents the first attempt to explore a semi-analytical CDOM retrieval algorithm for Landsat-8 multispectral imagery in shallow waters. SBOP was initially developed based on in situ spectroradiometer data. This study investigates its application to Landsat-8 OLI images and evaluates the effectiveness of the multi-spectral land-viewing images on the retrieval of CDOM absorption at a large number of lakes with significant variations in biogeochemical properties. Our approach strives to address the challenges of employing appropriate atmospheric correction, determining the influence of bottom reflectance, and refining a semi-analytical algorithm for bio-optical properties retrieval in optically shallow waters. Finally, 58 satellite images were processed and analyzed in Saginaw Bay, Lake Huron to better understand CDOM spatio-temporal dynamics and its associated driving factors.

2. Method

2.1. Study site

Saginaw Bay, Lake Huron was selected as our principal study site to develop our Landsat-8 methodologies (Fig. 1). A total of four data collection cruises were conducted in Saginaw Bay and vicinity to conduct in situ sampling focused on CDOM spatial variations. The field data generated from two of these collection cruises were used as algorithm validation data because their collection dates corresponded nicely to the overpass dates of select Landsat-8 satellite images. Fortunately, Saginaw Bay and the Saginaw River near their interface exhibit a wide range of CDOM absorption (440 nm), dynamically changing throughout the seasons. To compare with the satellite results, CDOM absorptions at 440 nm were from 0.5 m⁻¹ to 7.0 m⁻¹ with the mean values of 2.7 m⁻¹ according to our field recording. This variability makes this location perfect for testing if indeed satellite images can adequately capture CDOM seasonal dynamics in optically shallow waters. Generally, the major bottom sediments in Saginaw Bay were sand with the intermittent spot of aquatic plants and benthic algae. Moreover, the different landcover types surrounding Saginaw Bay also provide an opportunity to study the impact of various terrestrial CDOM export pathways into an aquatic ecosystem. For example, east coast of Saginaw Bay is dominated by agricultural cropland, while west coast of Saginaw Bay is dominated by a mixture of agriculture and forest. In addition, two major coastal wetland areas border Saginaw Bay and the Saginaw River, Wigwam Bay State Wildlife Area and Shiawassee National Wildlife Refuge. Saginaw River represents the largest river discharging into Saginaw Bay and has an overall length of 36 km and a watershed area of 22,260 sq. km². Also, there are several major agricultural drainage channels that discharge into Saginaw Bay.

2.2. Field data collection and laboratory measurements

Field data were acquired to verify image-based CDOM estimation results in Saginaw Bay and the Saginaw River. Sampling cruises were conducted on May 7, 2013, and May 7, 2015, in order to take water samples for CDOM absorption at 440 nm assessment and record associated water depths. A total of 24 water samples were collected in the Saginaw River and Saginaw Bay regions with amber Nalgene bottles. The samples were taken along four transects to ensure varied water depths and CDOM levels. Duplicate water samples were collected at four locations in order to conduct an uncertainty analysis. All water samples were immediately placed on ice to impede the degradation of

CDOM levels within the samples. A Satlantic HyperSAS hyperspectral radiometer was also used to measure water spectral data at each sampling location. Three sensors, including the downwelling irradiance sensor, sky radiance sensor, and total upwelling radiance sensor, were deployed to measure the remote sensing reflectance of water. These in situ spectral data were needed to aid in the examination of the atmospheric correction results of the satellite images. In addition, a hand-held Vexilar® depth sonar was used to measure the water bathymetry at 14 sampling locations during the May 7, 2015 sampling cruise. The bathymetry data of the other dates/locations were generated from the online public bathymetry contours and relative lake levels at the time the samples were taken (Michigan Geographic Data Library). The sampling depth ranges from 0.7 m to 4.0 m with a mean value of 1.8 m.

Water samples were processed in the laboratory within 6 h of their arrival to measure CDOM absorption. The first step was to filter the water sample with glass microfiber (GF/F) filters. These filtered samples were then pipetted into 1 cm diameter cuvettes and placed in a Cary® 60 UV-Vis Spectrophotometer to quantify CDOM absorption. Milli-Q water was used as a blank. The Cary® 60 generates absorbance A(λ) for wavelengths between 250 and 800 nm. Then an absorption coefficient a_{CDOM}(λ) was calculated via Eq. (1):

$$a_{CDOM}(\lambda) = \frac{\ln(10)}{L} \times A(\lambda) \tag{1}$$

where L represents the cuvette size used in the measurement. Following Miller and McKee (2004) the CDOM absorption coefficient at 440 nm (a_{CDOM}(440)) will hereafter represent CDOM levels.

2.3. Shallow water bio-optical properties (SBOP) algorithm

Shallow Water Bio-optical Properties (SBOP) algorithm was developed to retrieve CDOM absorption for both optically shallow and optically deep waters from in situ spectral data (Li et al., 2017). In this study, the SBOP algorithm was applied to Landsat-8 OLI images to estimate CDOM spatial and temporal dynamics in inland waters. In SBOP, Remote sensing reflectance (R_{rs}(λ)) derived from images was used to derive the below-surface remote sensing reflectance r_{rs} as shown in Eq. (2) (Lee et al., 1998):

$$r_{rs}(\lambda) = \frac{R_{rs}(\lambda)}{0.52 + 1.7R_{rs}(\lambda)} \tag{2}$$

The r_{rs}(λ) associated with all four wavelengths were utilized by SBOP algorithm to estimate CDOM absorption. Then r_{rs} is separated into two components, the water column contribution (r_{rs}^c) and bottom reflectance contribution (r_{rs}^b) as (r_{rs} = r_{rs}^c + r_{rs}^b). This separation is needed in order to address uncertainties associated with bottom effect. r_{rs}^c and r_{rs}^b can be expressed separately as shown in Eqs. (3) and (4) as:

$$r_{rs}^c = r_{rs}^{dp} (1 - e^{-D_c(a_t+b_b)H}) \tag{3}$$

$$r_{rs}^b = \frac{1}{\pi} \rho e^{-D_b(a_t+b_b)H} \tag{4}$$

H is the unknown factor for representing water depth. D_b and D_c are the empirical factors related to the sub-water surface photon path elongation (Lee et al., 1999). The r_{rs}^{dp} is the below surface remote sensing reflectance when the water depth is infinite which can be calculated as (Lee et al., 2013):

$$r_{rs}^{dp} = \left(0.089 + 0.125 \frac{b_b}{a_t + b_b} \right) \frac{b_b}{a_t + b_b} \tag{5}$$

a_t and b_b represent total absorption and backscattering of the water column at select wavelengths respectively. The total absorption a_t is separated into three absorption components; pure water a_w(λ), particulates a_p(λ) and CDOM a_{CDOM}(λ),

$$a_t(\lambda) = a_w(\lambda) + a_p(\lambda) + a_{CDOM}(\lambda) \tag{6}$$

The backscattering coefficient $b_b(\lambda)$ can be expressed as the sum of particle backscattering $b_{bp}(\lambda)$ and water backscattering $b_{bw}(\lambda)$:

$$b_b(\lambda) = b_{bw}(\lambda) + b_{bp}(\lambda) \quad (7)$$

where $b_{bp}(\lambda)$ could be applied to represent $a_p(\lambda)$ as (Zhu et al., 2013b):

$$a_p(\lambda) = 0.75 b_{bp}(\lambda) \quad (8)$$

ρ is the bottom reflectance which can be expressed as:

$$\rho(\lambda) = B\rho_{bottom}(\lambda) \quad (9)$$

The $\rho_{bottom}(\lambda)$ is the spectrum of the dominant bottom type (sand in our study sites) which is normalized by the signals at 555 nm (Lee et al., 2007b). B is the unknown factor which is the bottom reflectance at 555 nm. The B will be calculated as minimum in optically deep waters. The parameters in SBOP algorithm were selected as the global mean values. Utilizing these outlined parameters, the SBOP algorithm builds the modeled subsurface remote sensing reflectance (\widehat{r}_{rs}) by characterizing both the water column reflectance and bottom reflectance (Li et al., 2017).

The \widehat{r}_{rs} has four unknown variables: depth (H), bottom reflectance (B), particle backscattering (P) and CDOM absorption ($CDOM$). When applying SBOP algorithm to the multi-spectral images (e.g. Landsat-8), one dominant bottom type needs to be declared. The SBOP algorithm determines these four unknown variables through spectral optimization between the modeled below-surface remote sensing reflectance \widehat{r}_{rs} and satellite image derived below-surface remote sensing reflectance r_{rs} . Trust-Region method based on Taylor Approximation for nonlinear systems found in MATLAB was used to derive the unknown variables by minimizing the error expressed in Eq. (10) (Matlab, 2012; Powell, 1968):

$$error = \frac{\sqrt{\sum_{i=1}^N (r_{rs}(\lambda_i) - \widehat{r}_{rs}(\lambda_i))^2}}{\sqrt{\sum_{i=1}^N r_{rs}(\lambda_i)}} \quad (10)$$

In this error calculation, a minimum number of four separate wavelengths (r_{rs}) must be used.

2.4. Landsat-8 image processing and validation method

Landsat-8 satellite was launched in February 2013, with the addition of a new coastal blue band (443 nm). Its worldwide spatial coverage and high spatial resolution show promise for inland water CDOM monitoring. First, in Saginaw Bay, 84 images (path 20–21, row 29–30) since the launch of Landsat-8 until Feb 2016 were processed, excluding high ice or cloud cover (> 20%) during winter months. Most of the images were acquired between March and November in all four years. Of these, 26 processed images didn't have positive output from atmospheric correction due to high atmosphere aerosol scattering. Eventually, two images (May 1, 2013 and May 7, 2015) are closed to our field sampling dates and were used for validating against our field measurements. In addition, CDOM derived from 56 images were used to discuss the CDOM spatial-temporal dynamics.

The Level-1 images were further processed to retrieve the water-leaving remote sensing reflectance. ACOLITE software was used to perform an atmospheric correction and to extract water leaving radiance from TOA (top of atmospheric) radiance (Vanhellemont and Ruddick, 2014, 2015). The SWIR (Short-Wave Infrared) atmospheric correction method under Aerosol Correction options of the ACOLITE software was utilized due to the turbid inland water in our study sites (Vanhellemont and Ruddick, 2015). Other atmospheric correction parameters, including Rayleigh scale factor, atmospheric pressure and site elevation were set according to the weather and graphical location of study site. The cloud masking threshold values were set according to the cloud coverage condition in the images (0.0215 for normal day, 0.015 for the non-cloud day). After these correction efforts were completed, R_{rs} of land regions were masked out via the ACOLITE software

using normalized water index. Finally, the derived water R_{rs} is validated by our in situ R_{rs} measured by HyperSAS.

The SBOP algorithm used $R_{rs}(\lambda)$ values at 440 nm, 490 nm, 555 nm, and 640 nm, which is consistent with other semi-analytical algorithms (e.g. QAA-CDOM) (Zhu et al., 2014). The band centers of the four Landsat-8 bands used were coastal blue (443 nm), blue (482 nm), green (561 nm) and red (654 nm). Note that these band centers do not directly match the $R_{rs}(\lambda)$ wavelengths needed within the SBOP algorithm. Therefore, we interpolated $R_{rs}(\lambda)$ at the required wavelengths from Landsat-8 spectral data based on relative spectral response method (Barsi et al., 2014).

The CDOM estimation values were validated by comparing these image derived values to water sample lab measurements values. The image derived values were from a single pixel identified by the GPS location of field sampling. The comparison was made via the following statistical metrics: Root Mean Squared Error in log space (RMSE), R^2 (Type II-Regression), Mean Normalized Bias and Absolute Mean Error (AME). The calculation functions are following:

$$RMSE = \sqrt{\frac{\sum_{i=1}^n [\log(a_i^{est}) - \log(a_i^{obs})]^2}{n - 2}} \quad (11)$$

$$MNB = \frac{\sum_{i=1}^n \left(\frac{a_i^{est} - a_i^{obs}}{a_i^{obs}} \right)}{n} \quad (12)$$

$$AME = \frac{\sum_{i=1}^n \left(\left| \frac{a_i^{est} - a_i^{obs}}{a_i^{obs}} \right| \right)}{n} \quad (13)$$

where a_i^{est} is the image derived CDOM value and the a_i^{obs} is the laboratory-based CDOM value.

3. Results

3.1. Atmospheric correction validation

Image derived remote sensing reflectance (R_{rs}) after the atmospheric correction was validated by the HyperSAS measured field spectra. Two satellite images on May 7, 2013, and May 7, 2015 were time-synchronized with our two cruises in the Saginaw Bay, Lake Huron. In Fig. 2, full spectrum of field measured R_{rs} and four bands of image derived R_{rs} were compared. R_{rs} in three typical regions of Saginaw Bay, including Kawkawlin river plume region, near shore region, and inner bay region, were selected for the comparison. These three regions had descending different CDOM levels which are reflected by the different shapes of the spectrum curves. We found in all the three regions, image derived R_{rs} had comparable spectral shape and magnitude to corresponding in situ R_{rs} .

Image R_{rs} was statistically compared to in situ R_{rs} at four band center wavelengths from 25 field spectra (Table 1). The overall RMSE for all four wavelengths is 0.25. RMSE decreases towards longer wavelength and exhibits a slight overcorrection at shorter wavelength. For instance, the RMSE is 0.48 in 443 nm and 0.16 in 655 nm. Meanwhile, the atmospheric correction works better in the inner bay and Kawkawlin River region which had low bottom reflectance (Fig. 2). The bottom reflectance contributed in SWIR band may affect the atmospheric correction. All the image derived R_{rs} had slightly lower values than the field measured ones according to the AME values. Overall, the comparison results showed the ACOLITE software can be effectively applied in the turbid inland waters (Table 1).

3.2. CDOM estimation validation: Saginaw Bay

The CDOM absorption values derived from the Landsat-8 OLI images were validated with the laboratory measurement of CDOM in water samples. The results showed the SBOP algorithm can be

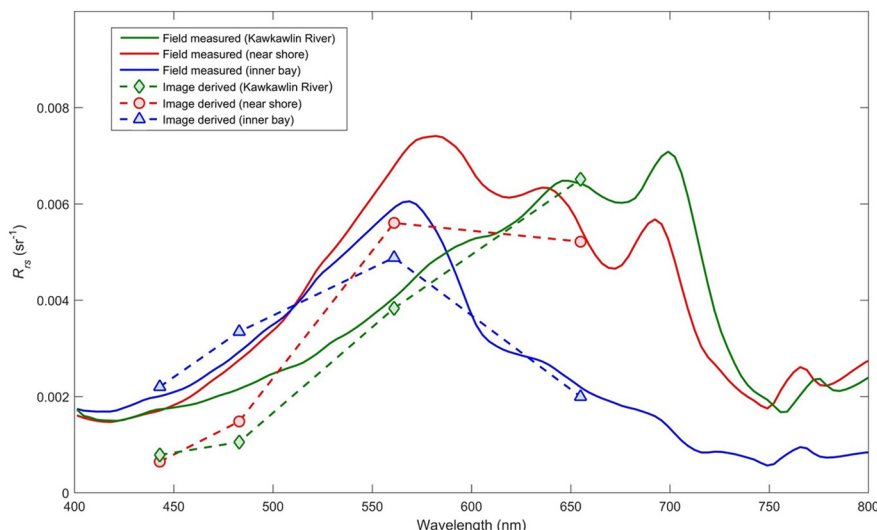


Fig. 2. The full spectrum of HyperSAS measured R_{rs} and image derived 4 bands R_{rs} in different regions of Saginaw Bay.

Table 1
The performances of atmospheric correction.

Method	RMSE	MNB	AME
Total	0.25	0.34	-0.33
443 nm	0.38	0.48	-0.45
483 nm	0.21	0.34	-0.32
561 nm	0.17	0.28	-0.28
655 nm	0.16	0.25	-0.24

Table 2
The performance of SBOP and QAA-CDOM algorithms via comparisons of both measured and image-derived $a_{CDOM}(440)$ in Saginaw Bay with 26 samples.

Method	RMSE	MNB	AME	R^2
SBOP	0.17	-0.12	0.22	0.87
QAA-CDOM	0.48	1.65	1.83	0.33

effectively applied to optically shallow waters and improve the accuracy of CDOM estimation (Table 2). A representative optically deep water semi-analytically algorithm (i.e. QAA-CDOM) was chosen to compare with the SBOP algorithm in the Saginaw Bay area (Zhu et al., 2014). Both SBOP and QAA-CDOM are semi-analytical algorithm with the same strategy for partitioning the absorption coefficient. The SBOP remarkably outperformed QAA-CDOM with respect to all four error metrics. The SBOP algorithm achieved a R^2 of 0.87, much higher than that of the QAA-CDOM algorithm ($R^2 = 0.33$). The substantially larger bias (MNB) and error (AME) of QAA-CDOM (MNB = 1.65 and AME = 1.82) showed that it overestimates CDOM levels dramatically.

To examine how errors change across sampling locations, $a_{CDOM}(440)$ derived from satellite images vs. field measured $a_{CDOM}(440)$ from field water samples were plotted in Fig. 3. These samples are located at a range of depth between 0.6 and 4 m, including both optically shallow and optically deep waters. The samples were categorized as shallow (depth < 1 m), medium (1 m < depth < 2 m) and deep waters (depth > 2 m) to evaluate algorithm performances in respect to bottom contribution. Generally, in Saginaw Bay, the shallow (depth < 1 m) and medium (1 m < depth < 2 m) sites had the bottom reflectance > 10% to the total water leaving radiance. In the shallow near shore regions with similar range of CDOM level, SBOP produced much better results than QAA-CDOM algorithm. In contrast, the largest errors of the QAA-CDOM algorithm resulted in these shallow areas. In optically shallow water sites, the underwater light reflected by

bottom sediments significantly contributes to water-leaving radiance, some of which is received by the satellite sensor. QAA-CDOM essentially does not consider bottom reflectance and includes it as a component of water column reflectance, which leads to the overestimation of CDOM absorptions. The higher the proportion of bottom reflectance included in the total water leaving reflectance, the higher the uncertainties resulting from QAA-CDOM. QAA-CDOM could produce a few accurate results in medium and deep depth waters. Almost half of the field sample locations in southern Saginaw Bay regions were classified as optically shallow water according to field measured depth (< 1.5 m). Our results show QAA-CDOM is not directly applicable to these shallow waters. On the contrary, the SBOP algorithm considers bottom reflectance in the water radiative transfer model and treats r_{rs} as a sum of both water column and bottom sediment reflectance. Moreover, bottom reflectance also involved in the total water leaving radiance in deep and clean waters (Li et al., 2017). So SBOP demonstrated a marked advantage over QAA-CDOM for estimating CDOM in a broad range of inland waters.

SBOP algorithm can be effectively applied to multi-spectral Landsat-8 images of inland waters. Moreover, Landsat-8 OLI imagery, particularly the four bands (443 nm, 482 nm, 561 nm, and 654 nm), provide sufficient spectral information to retrieve inland water CDOM levels. The spectral, radiometric and spatial resolutions of Landsat-8 OLI imagery are capable of achieving large-scale lake/estuary CDOM monitoring if a proper algorithm like SBOP is used. Two limitations of SBOP should be considered when implementing SBOP. First, the algorithm execution is computation-intensive because the spectral optimization method is used to derive the unknown radiative transfer variables in the CDOM retrieval. We are working on a fast SBOP algorithm to potentially reduce the computation. Second, SBOP algorithm performs better with the relatively homogenous bottom sediment type on individual Landsat-8 image for one algorithm execution. Because multiple spectral bands (4 bands) can only allow one endmember of bottom type in the model. Alternatively, the image can be divided into smaller tiles of similar bottom type and processed separately when the bottom type significantly varies within one image.

3.3. CDOM spatial gradient along the path from watershed to lake: Saginaw Bay vicinity

CDOM spatial distribution from the Saginaw River into Saginaw Bay in July 2013 and September 2015 is illustrated in Fig. 4. The lake water CDOM levels in Saginaw Bay displayed distinct spatial heterogeneity. The CDOM level significantly decreased from shallow near shore

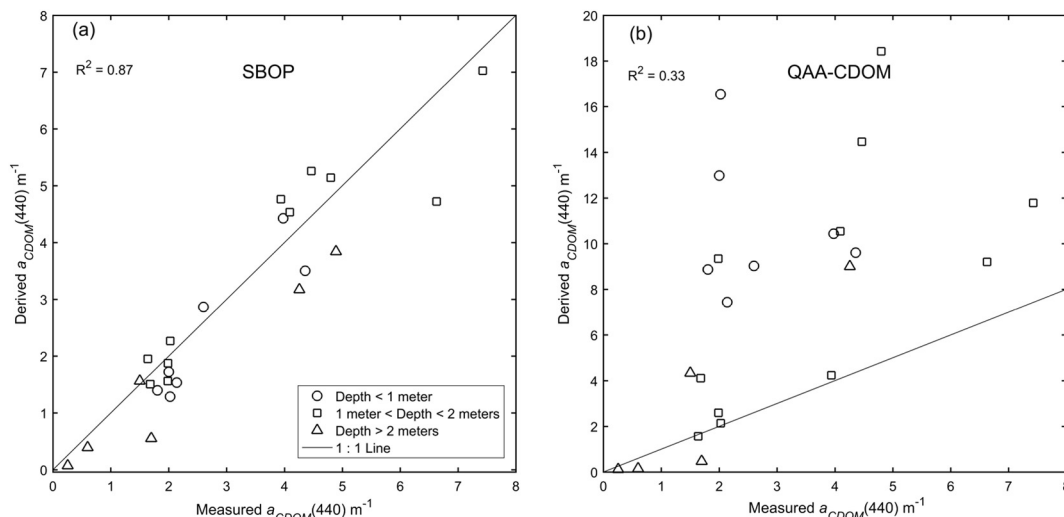


Fig. 3. Image derived vs measured $a_{CDOM}(440)$ from both SBOP and QAA-CDOM algorithms in Saginaw Bay. The larger symbol size indicated the higher error of the algorithm. Water samples were separated by the depths of field sampling sites.

regions to the deeper inner bay. CDOM was highest around the near shore regions where rivers and agricultural channels discharged into Saginaw Bay. CDOM levels in Saginaw River and channels were almost two times higher than that of Saginaw Bay. Specifically, Saginaw River had much higher CDOM levels than the other regions of Saginaw Bay for three non-winter seasons. Scenes in Fig. 4 strongly suggested that large amounts of CDOM were transported by this river system to the lake waters.

In order to more closely examine CDOM spatial distribution from the river into Saginaw Bay, CDOM absorption at 440 nm for five non-consecutive months across three years was plotted (Fig. 5a) along transect 3 shown in Fig. 1. The point locations along transect 3 were evenly distributed from the Saginaw River mouth out into the inner Bay at an interval of 1 km. Fig. 5a shows that CDOM absorption decreased almost by a factor of four in 10 km moving towards the inner bay. Similar data generated from September 2015 imagery for two additional transects (transect 1 & transect 2) is shown in Fig. 5b. Both transects are oriented from east to west, roughly perpendicular to transect 3. Transect 1 is located near the Saginaw River plume region while transect 2 is located in the inner Bay region. The CDOM levels along the near shore transect (transect 1) were generally two times higher than

CDOM levels within the deeper inner bay (transect 2).

3.4. CDOM spatial gradient and surrounding terrestrial environment

Clearly CDOM levels within aquatic ecosystems are significantly affected by the terrestrial sources of organic matter. To further analyze how terrestrial CDOM migrates to Saginaw Bay waters, we compared water CDOM levels in areas influenced by different landcover types. In Fig. 6, one high CDOM level area was found along the north coast of Saginaw Bay, this was also visible in Fig. 4a-4b. This area of elevated CDOM was associated with the Wigwam Bay State Wildlife Area, which is dominated by coastal marsh plant species (Burton et al., 2002; Uzarski et al., 2004). Fig. 6 shows how significantly carbon associated with these coastal wetlands influences CDOM in the near shore environment. The average CDOM absorption in the wetland influenced areas was 1.70 m^{-1} while the average of waters bordered by mixed agri-forest regions was 0.85 m^{-1} . Moreover, the results in Figs. 4 and 6 showed the east coast of Saginaw Bay had relatively higher CDOM levels than the west coast. The east Bay shore had a higher percentage of agricultural farmland. However, the west Bay shore was dominated by mixed agriculture and forest. Another large wetland area along the

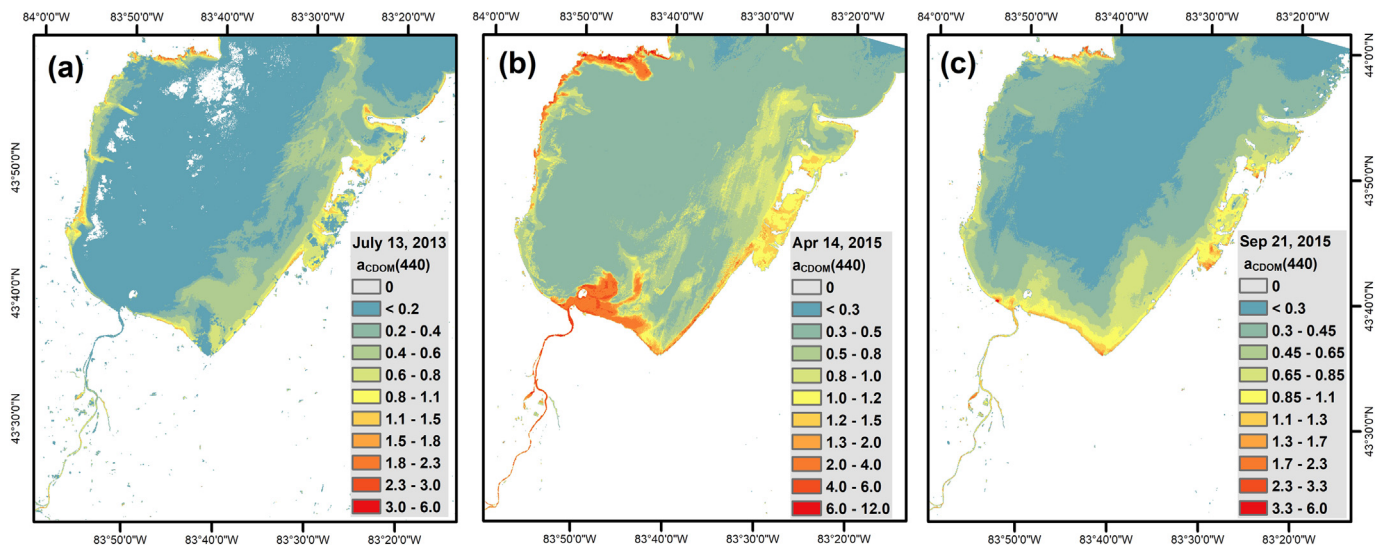


Fig. 4. Spatial distribution of $a_{CDOM}(440)$ across two different seasons in Saginaw Bay.

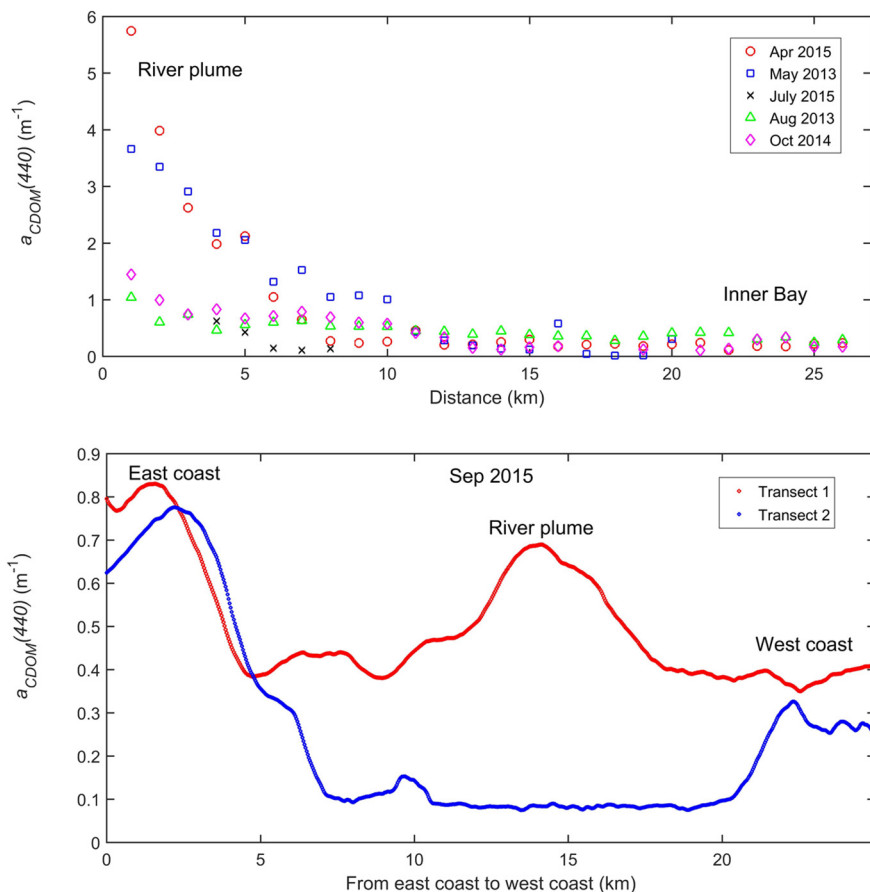


Fig. 5. (a) Decreasing $a_{CDOM}(440)$ across five non-consecutive months from the Saginaw River to the inner bay along transect 3 (see Fig. 1). (b) A comparison of varied $a_{CDOM}(440)$ along transects 1 & 2 derived from September 2015 image.

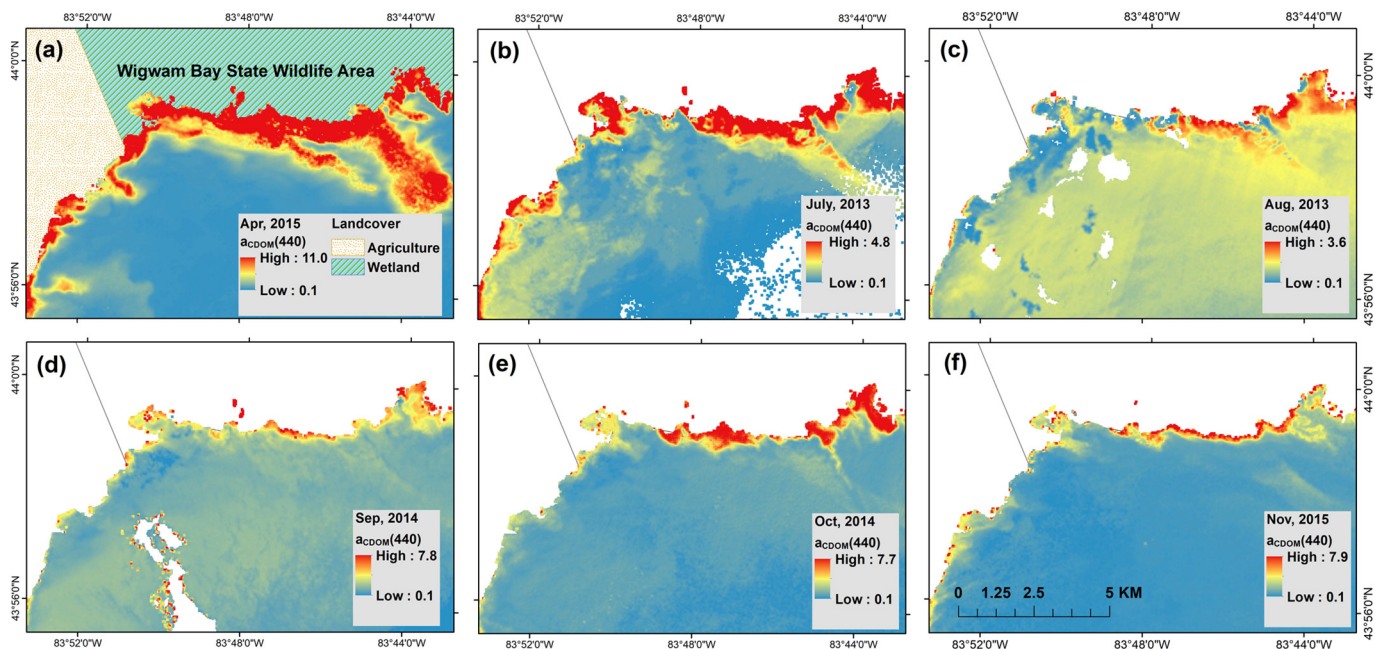


Fig. 6. $a_{CDOM}(440)$ spatial patterns in six different months in the north coast of Saginaw Bay. $a_{CDOM}(440)$ is higher for waters adjacent to the wetland than water near agriculture.

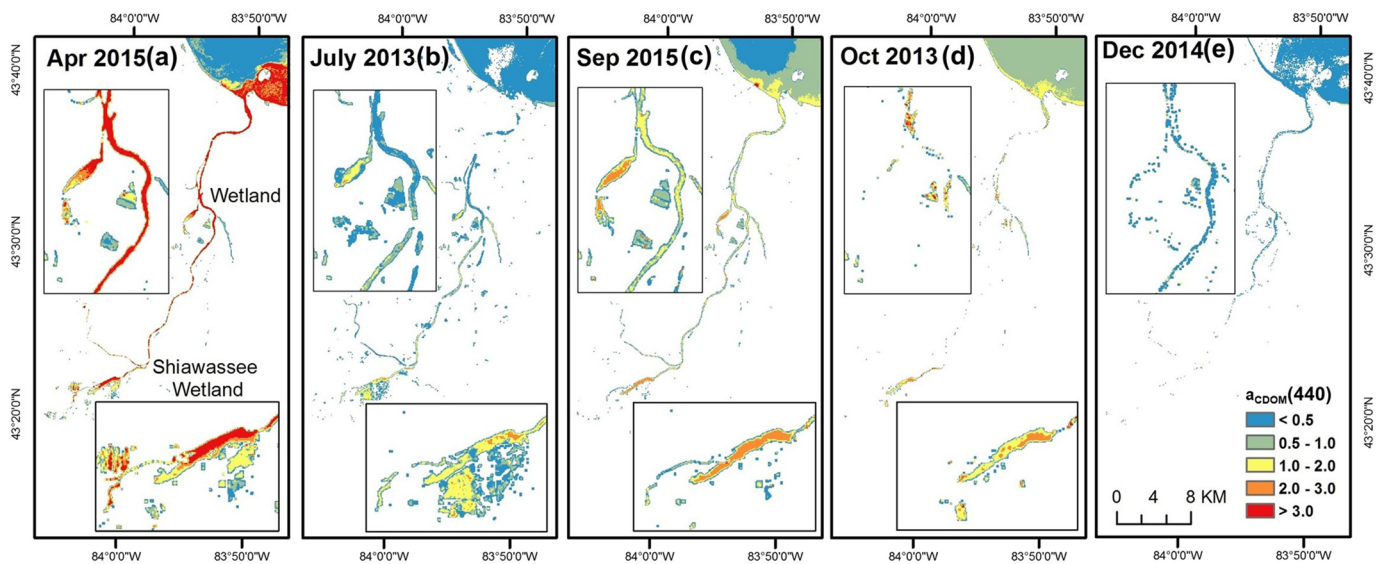


Fig. 7. Comparison of $a_{CDOM}(440)$ associated with adjacent landcover types and seasonality in the Saginaw River region. Spring had higher $a_{CDOM}(440)$ than the other seasons.

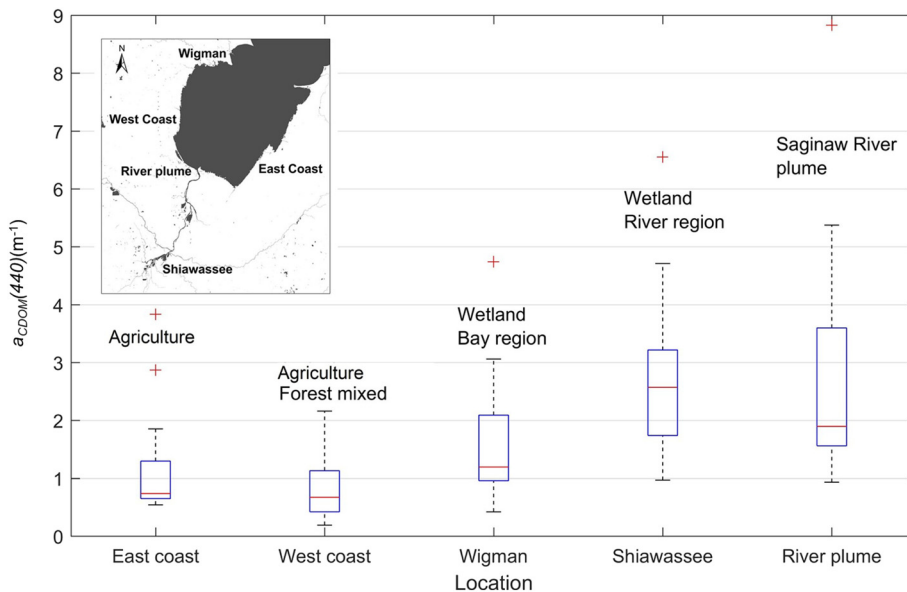


Fig. 8. Boxplot diagrams show the 75th, median and 25th percentile of mean $a_{CDOM}(440)$ associated with 5 different landcover types regions.

shoreline of the Saginaw River is the Shiawassee National Wildlife Refuge (Fig. 7). Similar to Saginaw Bay, river CDOM levels near the Shiawassee wetland region were significantly higher than surrounding regions.

To further explore how biogeography influences CDOM in aquatic ecosystems, mean CDOM levels along the east coast (predominantly agriculture), west coast (agri-forest mixed), Wigman Bay (wetland), Shiawassee wetlands (upstream Saginaw River) and Saginaw River plume regions were plotted (Fig. 8). As outlined above, waters associated with coastal wetlands had the highest CDOM levels compared to that found in the agriculture and mixed agri-forest regions. The Shiawassee region had higher CDOM levels than that of Wigman Bay, as might be expected due to the much larger size of the Shiawassee wetland area (Wigman = 3.64 km², Shiawassee = 40 km²) and dilution of CDOM levels by Lake Huron. Lakes in the agricultural cropland regions had higher CDOM levels compare to the lakes in the mixed agri-forest regions. The highest CDOM levels were again associated with the Saginaw River plume which receives contributions from a wide variety of

landcover types including wetlands and agricultural croplands.

3.5. Aggregated CDOM statistics based on seasonal phenology in Saginaw Bay

The path/row designation and associated dates for all processed Landsat-8 images of the Saginaw Bay (< 20% cloud coverage) were plotted in Fig. 9a. These images spread well over time to monitor CDOM from March to the November. As discussed above, high levels of cloud coverage and ice coverage limit the derivation of CDOM in late fall through winter. The CDOM levels in the Saginaw Bay derived from satellite images showed clearly seasonal dynamics. For instance, the CDOM values were illustrated in five different months had different CDOM levels (Fig. 7). Fig. 9b provides boxplot diagrams showing the 75th, median and 25th percentile of mean CDOM levels associated with different seasons. These mean CDOM values were derived in three different regions of Saginaw Bay through the ArcGIS zonal statistics for all the available CDOM results. Peak CDOM levels occurred in the

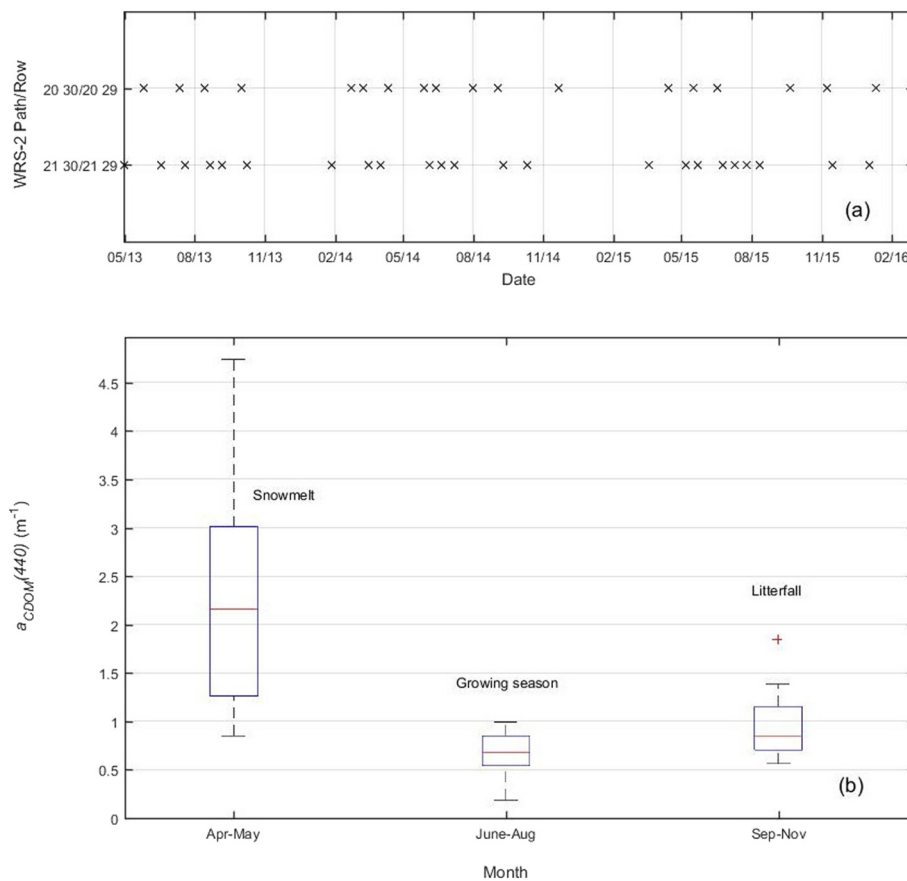


Fig. 9. (a) The path/row designation and associated dates for all available Landsat-8 images of Saginaw Bay study area with low ice and cloud coverage (< 20%) from 2013 to 2016. (b) Boxplot draws the 75th, median and 25th percentile of $a_{CDOM}(440)$ across three seasons.

spring associated with snow melt and associated spring runoff (e.g. April 2015), and were two times higher than that of the other three seasons. This product coincides with the recently reported riverine CDOM dynamics in Michigan, particularly high spring CDOM fluxes, due to decomposition of agricultural residues and transport processes driven by snow melting (Qiao et al., 2017). A secondary peak of CDOM level is evident in early fall and is associated with litterfall and the availability of crop residues on the landscape (e.g. September 2015, October 2013). The summer generally had the lower CDOM levels compared to the spring and fall (e.g. July 2013). Meanwhile, the winter months generally displayed the lowest CDOM values of the year. CDOM seasonal dynamics is clearly related to the terrestrial CDOM supplies linked to seasonal changes to landcover and agricultural phenological cycles.

4. Discussions

4.1. Terrestrial CDOM inputted to lake waters via river systems

The CDOM spatial patterns derived from satellite images clearly suggested that CDOM in the lake waters is significantly affected by terrestrial CDOM input via the Saginaw River. As the elevated CDOM levels associated with the discharge plume of the Saginaw River indicate, allochthonous CDOM from terrestrial sources is an important CDOM source for lakes (Kelly et al., 2014; Kritzberg et al., 2004). Often, the major allochthonous CDOM source originates from watershed soil carbon leaching and its subsequent transport to the aquatic environment (Kalbitz et al., 2000; Kindler et al., 2011; Major et al., 2010). Inland river systems provide the network for this transport of terrestrial CDOM to lakes and coastal ocean waters (Findlay et al., 2001). Similar as in Saginaw Bay, terrigenous CDOM was observed to be one or two

magnitudes higher than the autochthonous carbon sources in the Chesapeake Bay and Lake Tuscaloosa (Rochelle-Newall and Fisher, 2002; Vähätalo and Wetzel, 2004). It is concurred in our study that the allochthonous CDOM in the Saginaw River was almost two times higher than the CDOM in inner Bay region. The successful monitoring of CDOM spatial distribution using high spatial resolution remote sensing is significant in that it helps understand the degradation and dilution under mixing process at land-water interface and assess the bio-optical impact of terrestrially derived CDOM on lake ecosystem (Palmer et al., 2015; Toming et al., 2016).

4.2. Lake CDOM spatial distributions affected by terrestrial biogeography

Our results indicate the Landsat-8 images are indeed applicable to the examination of the influence of biogeography on CDOM spatial variations. Previous studies confirmed the surrounding carbon sources from processes like plant material decay and soil carbon leaching contribute greatly to CDOM levels in river and lake environments (Boyle et al., 2009; Williams et al., 2010). Different landcover types play an important role in determining CDOM transportation from land to water (Butman and Raymond, 2011). The CDOM levels in our studies showed that the lake areas influenced by wetlands had the highest level compared to the agricultural and mixed agri-forest regions across all seasons. The organic matter directly leached from persistent senescent wetland plant biomass to water was observed as an important CDOM source in the lake water in a previous study (Maie et al., 2006).

However, in the water regions receiving carbon from inland agriculture and forest, CDOM generally is routed through longer paths and often CDOM levels are reduced via degradation and dilution. In the Saginaw Bay regions, our results showed that CDOM level exported from agriculture dominant regions were slightly higher in from mixed

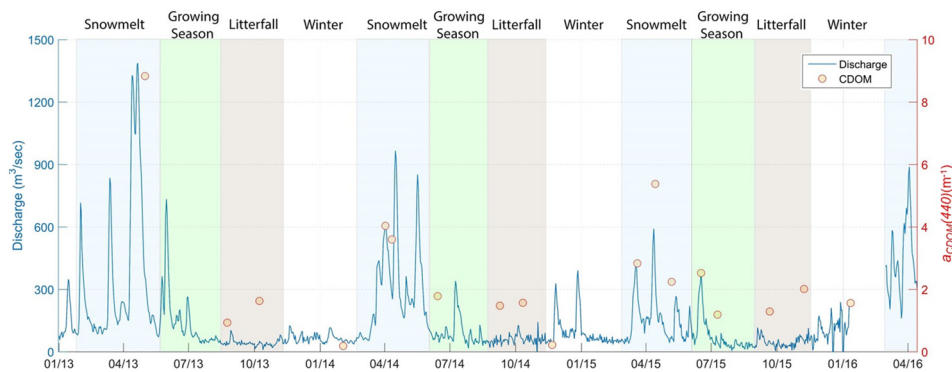


Fig. 10. Landsat image derived $a_{CDOM}(440)$ versus discharge at the Saginaw River mouth from January 2013 to April 2016.

agri-forest regions. This is likely attributed to the fact that crop residues remaining in agricultural fields after harvest supply more abundant biomass in the topsoil than that of forest in the Saginaw Bay regions (Boyer and Groffman, 1996; Laudon et al., 2011). In all, CDOM spatial distribution is modulated by both landcover type and human land use practices, such as farming. The CDOM monitored via Landsat 8 could provide insightful information that helps improve our understanding of the effects of land use practices and land management on the terrestrial carbon export to the lakes and rivers (Yallop and Clutterbuck, 2009).

4.3. Lake CDOM seasonal dynamics were affected by hydrological activities

In order to further explore CDOM dynamics associated with the Saginaw River, CDOM levels in Saginaw River mouth were compared with its discharge (Fig. 10). The comparison aims to investigate the hydrology effect to further explain the seasonal dynamics of terrestrial CDOM export to Saginaw Bay. Large amounts of CDOM were exported from the land (allochthonous) to the river as the channel gathered runoff from watershed during periods of high discharge (Fig. 10). The highest riverine CDOM level shown in Fig. 10 occurred in April 2013, synchronized with the highest discharge across the four-year period under study. Similarly, it was commonly reported that elevated CDOM level is associated with the periods of high discharge (Battin et al., 2008; Evans et al., 2005; Hornberger et al., 1994). This phenomenon was often observed when the soil has stored abundant decomposed materials (e.g. long dry period/snow cover) before the rainfall. In the early spring, large amounts of soil carbon are mobilized and are finally exported to the aquatic ecosystem carried by the snowmelt water and rainfall water (Ågren et al., 2010; Haei et al., 2010; Qiao et al., 2017). All these contribute to the highest water CDOM in the spring. During the fall, breakdown of fresh litterfall would cause relatively high soil carbon levels (Kalbitz and Kaiser, 2008). It is also worth to notice that the low CDOM during the summer time may be caused by the seasonal dynamics of the photobleaching and microbial loop (Hart et al., 2000; Del Vecchio and Blough, 2004).

Interestingly, an anomaly occurred during the winter of 2015, for its CDOM levels were elevated compared to other winters shown. This pattern was likely caused by historically warm winter temperatures in 2015, leading to both the Saginaw River and Saginaw Bay being ice free for an abnormally long period. We assume that an unfrozen river and watershed acts as a better conduit for CDOM (Jan, 2016) than what is typically expected during winter months. The river systems could more effectively transport the terrestrial CDOM to Saginaw Bay. Our CDOM absorption derived from the satellite images illustrates that land-water carbon exchange was significantly affected by the hydrology.

5. Conclusions

This study presented an application of a new semi-analytical algorithm SBOP, previously validated with field spectroradiometer data, to

Landsat-8 OLI imagery for improving CDOM retrieval in optically shallow inland waters. The investigation was supported by 58 satellite images and in-situ field measurements collected over varying seasons across multiple years. Our research concludes the following:

- 1) The SBOP algorithm performance on CDOM estimation was robust and consistent across a broad range of CDOM absorption, highlighting the transferability and scalability of our methodology. Separating bottom reflectance from other radiance pathways in the SBOP algorithm remarkably improved the estimation accuracy of CDOM for inland optically shallow waters. The RMSE was reduced to one third of a semi-analytical deep-water CDOM algorithm.
- 2) Landsat-8 OLI imagery provides sufficient spatial (30 m), spectral (i.e. 443 nm, 482 nm, 561 nm, and 654 nm) and radiometric resolution required for retrieving CDOM levels for both optically shallow and deep inland waters. It enables high spatial resolution mapping of CDOM gradient from lower reaches of a river, shoreline, to open water, which is strongly connected to the ambient environment. Meanwhile, the temporal frequency of the CDOM monitoring could be further improved by adding other satellite sensors, such as Sentinel-2. Consequently, monitoring the allochthonous CDOM transportation from terrestrial to aquatic ecosystems will improve our understanding of land-water carbon cycles.
- 3) CDOM seasonal variation assessment was benefited by the high spatial and temporal resolution monitoring. Detailed CDOM spatial pattern at the land-water interface contributed to the understanding of the magnitude that terrestrial CDOM loading couples with the type and abundance of the terrestrial plant sources in adjacent ecosystems. In Saginaw Bay, CDOM level released from landscape exhibits a descending order from wetland, agriculture, to agriculture-forest mixed landcover. Moreover, a complete Landsat-8 time series of CDOM over three-year demonstrated a good synchronization to the river discharge and reveals the spatial pattern of pronounced CDOM peaks during snowmelt. These findings suggest potential for quantitative estimation of CDOM loading from land to water at large scale.

Acknowledgment

This research was supported by two collaborative grants from the National Science Foundation (Grant #: 1025547; Grant #: 1230261) and UMass Faculty Research Grant. All authors appreciate the constructive feedbacks and editorial suggestions from three reviewers and the editor. The paper is contribution No. 94 of the Institute for Great Lakes Research, Central Michigan University.

References

- Ågren, A., Haei, M., Kohler, S., Bishop, K., Laudon, H., 2010. Regulation of stream water dissolved organic carbon (DOC) concentrations during snowmelt: the role of

- discharge, winter climate and memory effects. *Biogeosciences* 7, 2901–2913.
- Allen, G.H., Pavelsky, T.M., 2015. Patterns of river width and surface area revealed by the satellite-derived North American River width data set. *Geophys. Res. Lett.* 42, 395–402.
- Barsi, J.A., Lee, K., Kvaran, G., Markham, B.L., Pedely, J.A., 2014. The spectral response of the Landsat-8 operational land imager. *Remote Sens.* 6, 10232–10251.
- Bastviken, D., Tranvik, L.J., Downing, J.A., Crill, P.M., Enrich-Prast, A., 2011. Freshwater methane emissions offset the continental carbon sink. *Science* 331 (50–50).
- Battin, T.J., Kaplan, L.A., Findlay, S., Hopkinson, C.S., Marti, E., Packman, A.I., Newbold, J.D., Sabater, F., 2008. Biophysical controls on organic carbon fluxes in fluvial networks. *Nat. Geosci.* 1, 95–100.
- Battin, T.J., Luysaert, S., Kaplan, L.A., Aufdenkampe, A.K., Richter, A., Tranvik, L.J., 2009. The boundless carbon cycle. *Nat. Geosci.* 2, 598–600.
- Boyer, J., Groffman, P., 1996. Bioavailability of water extractable organic carbon fractions in forest and agricultural soil profiles. *Soil Biol. Biochem.* 28, 783–790.
- Boyle, E.S., Guerrero, N., Thiallet, A., Vecchio, R.D., Blough, N.V., 2009. Optical properties of humic substances and CDOM: relation to structure. *Environ. Sci. Technol.* 43, 2262–2268.
- Brezonik, P.L., Olmanson, L.G., Finlay, J.C., Bauer, M.E., 2015. Factors affecting the measurement of CDOM by remote sensing of optically complex inland waters. *Remote Sens. Environ.* 157, 199–215.
- Burton, T.M., Stricker, C.A., Uzarski, D.G., 2002. Effects of plant community composition and exposure to wave action on invertebrate habitat use of Lake Huron coastal wetlands. *Lakes Reserv. Res. Manag.* 7, 255–269.
- Butman, D., Raymond, P.A., 2011. Significant efflux of carbon dioxide from streams and rivers in the United States. *Nat. Geosci.* 4, 839–842.
- Butman, D., Stackpoole, S., Stets, E., McDonald, C.P., Clow, D.W., Striegl, R.G., 2016. Aquatic carbon cycling in the conterminous United States and implications for terrestrial carbon accounting. *Proc. Natl. Acad. Sci.* 113, 58–63.
- Carder, K.L., Chen, F., Lee, Z., Hawes, S., Kamykowski, D., 1999. Semianalytic moderate-resolution imaging spectrometer algorithms for chlorophyll *a* and absorption with bio-optical domains based on nitrate-depletion temperatures. *J. Geophys. Res. Oceans* 104, 5403–5421.
- Chen, J., Zhu, W.-N., Tian, Y.Q., Yu, Q., 2017. Estimation of colored dissolved organic matter from Landsat-8 imagery for complex inland water: case study of Lake Huron. *IEEE Trans. Geosci. Remote Sens.* 55, 2201–2212.
- Cole, J.J., Carpenter, S.R., Pace, M.L., Van de Bogert, M.C., Kitchell, J.L., Hodgson, J.R., 2006. Differential support of lake food webs by three types of terrestrial organic carbon. *Ecol. Lett.* 9, 558–568.
- Cole, J.J., Prairie, Y.T., Caraco, N.F., McDowell, W.H., Tranvik, L.J., Striegl, R.G., Duarte, C.M., Kortelainen, P., Downing, J.A., Middelburg, J.J., 2007. Plumbing the global carbon cycle: integrating inland waters into the terrestrial carbon budget. *Ecosystems* 10, 172–185.
- Cuthbert, Iain D., Del Giorgio, Paul, 1992. Toward a standard method of measuring color in freshwater. *Limnol. Oceanogr.* 37 (6), 1319–1326.
- Davidson, E.A., Figueiredo, R.O., Markewitz, D., Aufdenkampe, A.K., 2010. Dissolved CO₂ in small catchment streams of eastern Amazonia: a minor pathway of terrestrial carbon loss. *J. Geophys. Res. Biogeosci.* 115.
- Del Vecchio, Rossana, Blough, Neil V., 2004. Spatial and seasonal distribution of chromophoric dissolved organic matter and dissolved organic carbon in the middle Atlantic bight. *Mar. Chem.* 89 (1–4), 169–187.
- Diehl, S., 2002. Phytoplankton, light, and nutrients in a gradient of mixing depths: theory. *Ecology* 83, 386–398.
- Evans, C., Monteith, D., Cooper, D., 2005. Long-term increases in surface water dissolved organic carbon: observations, possible causes and environmental impacts. *Environ. Pollut.* 137, 55–71.
- Findlay, S., Quinn, J.M., Hickey, C.W., Burrell, G., Downes, M., 2001. Effects of land use and riparian flowpath on delivery of dissolved organic carbon to streams. *Limnol. Oceanogr.* 46, 345–355.
- Haei, M., Öquist, M.G., Buffam, I., Ågren, A., Blomkvist, P., Bishop, K., Ottosson Löfvenius, M., Laudon, H., 2010. Cold winter soils enhance dissolved organic carbon concentrations in soil and stream water. *Geophys. Res. Lett.* 37.
- Hart, Deborah R., Stone, Lewi, Berman, Tom, 2000. Seasonal dynamics of the Lake Kinneret food web: the importance of the microbial loop. *Limnol. Oceanogr.* 45 (2), 350–361.
- Hoge, F.E., Lyon, P.E., 1996. Satellite retrieval of inherent optical properties by linear matrix inversion of oceanic radiance models: an analysis of model and radiance measurement errors. *J. Geophys. Res.* 101, 16631–16616, 16648.
- Hornberger, G., Bencala, K., McKnight, D., 1994. Hydrological controls on dissolved organic carbon during snowmelt in the Snake River near Montezuma, Colorado. *Biogeochemistry* 25, 147–165.
- Jonsson, A., Karlsson, J., Jansson, M., 2003. Sources of carbon dioxide supersaturation in Clearwater and humic lakes in northern Sweden. *Ecosystems* 6, 224–235.
- Kahru, M., Mitchell, B.G., 2001. Seasonal and nonseasonal variability of satellite-derived chlorophyll and colored dissolved organic matter concentration in the California current. *J. Geophys. Res. Oceans* 106, 2517–2529.
- Kalbitz, K., Kaiser, K., 2008. Contribution of dissolved organic matter to carbon storage in forest mineral soils. *J. Plant Nutr. Soil Sci.* 171, 52–60.
- Kalbitz, K., Solinger, S., Park, J.H., Michalzik, B., Matzner, E., 2000. Controls on the dynamics of dissolved organic matter in soils: a review. *Soil Sci.* 165, 277–304.
- Kelly, P.T., Solomon, C.T., Weidel, B.C., Jones, S.E., 2014. Terrestrial carbon is a resource, but not a subsidy, for lake zooplankton. *Ecology* 95, 1236–1242.
- Keith, Darryl J., Lunetta, Ross S., Schaeffer, Blake A., 2016. Optical models for remote sensing of colored dissolved organic matter absorption and salinity in new England, Middle Atlantic and Gulf Coast Estuaries USA. *Remote Sens.* 8 (4), 283.
- Kindler, R., Siemens, J., Kaiser, K., Walmsley, D.C., Bernhofer, C., Buchmann, N., Cellier, P., Eugster, W., Gleixner, G., Grünwald, T., 2011. Dissolved carbon leaching from soil is a crucial component of the net ecosystem carbon balance. *Glob. Chang. Biol.* 17, 1167–1185.
- Kritzer, E.S., Cole, J.J., Pace, M.L., Granéli, W., Bade, D.L., 2004. Autochthonous versus allochthonous carbon sources of bacteria: results from whole-lake ¹³C addition experiments. *Limnol. Oceanogr.* 49, 588–596.
- Kutser, T., Pierson, D.C., Kallio, K.Y., Reinart, A., Sobek, S., 2005. Mapping lake CDOM by satellite remote sensing. *Remote Sens. Environ.* 94, 535–540.
- Kutser, T., Verpoorter, C., Paavel, B., Tranvik, L.J., 2015. Estimating lake carbon fractions from remote sensing data. *Remote Sens. Environ.* 157, 138–146.
- Kutser, T., Casal Pascual, G., Barbosa, C., Paavel, B., Ferreira, R., Carvalho, L., Toming, K., 2016. Mapping inland water carbon content with Landsat 8 data. *Int. J. Remote Sens.* 37, 2950–2961.
- Laudon, H., Berggren, M., Ågren, A., Buffam, I., Bishop, K., Grabs, T., Jansson, M., Köhler, S., 2011. Patterns and dynamics of dissolved organic carbon (DOC) in boreal streams: the role of processes, connectivity, and scaling. *Ecosystems* 14, 880–893.
- Le, C., Hu, C., Cannizzaro, J., English, D., Muller-Karger, F., Lee, Z., 2013. Evaluation of chlorophyll-*a* remote sensing algorithms for an optically complex estuary. *Remote Sens. Environ.* 129, 75–89.
- Lee, Z., Carder, K.L., Mobley, C.D., Steward, R.G., Patch, J.S., 1998. Hyperspectral remote sensing for shallow waters. I. A semianalytical model. *Appl. Opt.* 37, 6329–6338.
- Lee, Z., Carder, K.L., Mobley, C.D., Steward, R.G., Patch, J.S., 1999. Hyperspectral remote sensing for shallow waters. 2. Deriving bottom depths and water properties by optimization. *Appl. Opt.* 38, 3831–3843.
- Lee, Z., Carder, K.L., Arnone, R.A., 2002. Deriving inherent optical properties from water color: a multiband quasi-analytical algorithm for optically deep waters. *Appl. Opt.* 41, 5755–5772.
- Lee, Z., Carder, K., Arnone, R., He, M., 2007a. Determination of primary spectral bands for remote sensing of aquatic environments. *Sensors* 7, 3428–3441.
- Lee, Z., Casey, B., Arnone, R., Weidemann, A., Parsons, R., Montes, M.J., Gao, B.-C., Goode, W., Davis, C., Dye, J., 2007b. Water and bottom properties of a coastal environment derived from Hyperion data measured from the EO-1 spacecraft platform. *J. Appl. Remote Sens.* 1 (011502-011502-011516).
- Lee, Z., Weidemann, A., Arnone, R., 2013. Combined Effect of Reduced Band Number and Increased Bandwidth on Shallow Water Remote Sensing: The Case of WorldView 2.
- Li, J., Yu, Q., Tian, Y.Q., Becker, B.L., 2017. Remote sensing estimation of colored dissolved organic matter (CDOM) in optically shallow waters. *ISPRS J. Photogramm. Remote Sens.* 128, 98–110.
- Maie, N., Jaffé, R., Miyoshi, T., Childers, D.L., 2006. Quantitative and qualitative aspects of dissolved organic carbon leached from senescent plants in an oligotrophic wetland. *Biogeochemistry* 78, 285–314.
- Major, J., Lehmann, J., Rondon, M., Goodale, C., 2010. Fate of soil-applied black carbon: downward migration, leaching and soil respiration. *Glob. Chang. Biol.* 16, 1366–1379.
- Mannino, A., Russ, M.E., Hooker, S.B., 2008. Algorithm development and validation for satellite-derived distributions of DOC and CDOM in the US middle Atlantic bight. *J. Geophys. Res. Oceans* 113.
- Matlab, M., 2012. *The Language of Technical Computing. The MathWorks, Inc.* <http://www.mathworks.com>.
- Matsuoka, A., Hooker, S., Bricaud, A., Gentili, B., Babin, M., 2013. Estimating absorption coefficients of colored dissolved organic matter (CDOM) using a semi-analytical algorithm for southern Beaufort Sea waters: application to deriving concentrations of dissolved organic carbon from space. *Biogeosciences* 10, 917–927.
- Miller, R.L., McKee, B.A., 2004. Using MODIS Terra 250 m imagery to map concentrations of total suspended matter in coastal waters. *Remote Sens. Environ.* 93, 259–266.
- Olmanson, L.G., Brezonik, P.L., Finlay, J.C., Bauer, M.E., 2016. Comparison of Landsat 8 and Landsat 7 for regional measurements of CDOM and water clarity in lakes. *Remote Sens. Environ.* 185, 119–128.
- O'Reilly, J.E., Maritorena, S., Mitchell, B.G., Siegel, D.A., Carder, K.L., Garver, S.A., Kahru, M., McClain, C., 1998. Ocean color chlorophyll algorithms for SeaWiFS. *J. Geophys. Res. Oceans* 103, 24937–24953.
- Pahlevan, N., Lee, Z., Wei, J., Schaaf, C.B., Schott, J.R., Berk, A., 2014. On-orbit radiometric characterization of OLI (Landsat-8) for applications in aquatic remote sensing. *Remote Sens. Environ.* 154, 272–284.
- Palmer, S.C., Kutser, T., Hunter, P.D., 2015. Remote sensing of inland waters: challenges, progress and future directions. *Remote Sens. Environ.* 157, 1–8.
- Powell, M.J., 1968. A FORTRAN Subroutine for Solving Systems of Nonlinear Algebraic Equations. Atomic Energy Research Establishment, Harwell (England).
- Qiao, H., Tian, Y.Q., Yu, Q., Carrick, H.J., Francek, M., Li, J., 2017. Snowpack enhanced dissolved organic carbon export during a variety of hydrologic of events in an agricultural landscape, Midwestern USA. *Agric. For. Meteorol.* 246, 31–41.
- Raymond, P.A., Hartmann, J., Lauerwald, R., Sobek, S., McDonald, C., Hoover, M., Butman, D., Striegl, R., Mayorga, E., Humborg, C., 2013. Global carbon dioxide emissions from inland waters. *Nature* 503, 355.
- Rochelle-Newall, E., Fisher, T., 2002. Chromophoric dissolved organic matter and dissolved organic carbon in Chesapeake Bay. *Mar. Chem.* 77, 23–41.
- Roulet, N., Moore, T.R., 2006. Environmental chemistry: Browning the waters. *Nature* 444, 283–284.
- Roy, D.P., Wulder, M., Loveland, T., Woodcock, C., Allen, R., Anderson, M., Helder, D., Irons, J., Johnson, D., Kennedy, R., 2014. Landsat-8: science and product vision for terrestrial global change research. *Remote Sens. Environ.* 145, 154–172.
- Shanmugam, P., 2011. New models for retrieving and partitioning the colored dissolved organic matter in the global ocean: implications for remote sensing. *Remote Sens. Environ.* 115, 1501–1521.
- Tian, Y.Q., Yu, Q., Feig, A.D., Ye, C., Blunden, A., 2013. Effects of climate and land-surface processes on terrestrial dissolved organic carbon export to major US coastal

- rivers. *Ecol. Eng.* 54, 192–201.
- Toming, K., Kutser, T., Laas, A., Sepp, M., Paavel, B., Nöges, T., 2016. First experiences in mapping lake water quality parameters with Sentinel-2 MSI imagery. *Remote Sens.* 8, 640.
- Tranvik, L.J., Downing, J.A., Cotner, J.B., Loiselle, S.A., Striegl, R.G., Ballatore, T.J., Dillon, P., Finlay, K., Fortino, K., Knoll, L.B., 2009. Lakes and reservoirs as regulators of carbon cycling and climate. *Limnol. Oceanogr.* 54, 2298–2314.
- Uzarski, D., Burton, T., Genet, J., 2004. Validation and performance of an invertebrate index of biotic integrity for Lakes Huron and Michigan fringing wetlands during a period of lake level decline. *Aquat. Ecosyst. Health Manag.* 7, 269–288.
- Vähätalo, A.V., Wetzel, R.G., 2004. Photochemical and microbial decomposition of chromophoric dissolved organic matter during long (months–years) exposures. *Mar. Chem.* 89, 313–326.
- Vanhellemont, Q., Ruddick, K., 2014. Turbid wakes associated with offshore wind turbines observed with Landsat 8. *Remote Sens. Environ.* 145, 105–115.
- Vanhellemont, Q., Ruddick, K., 2015. Advantages of high quality SWIR bands for ocean colour processing: examples from Landsat-8. *Remote Sens. Environ.* 161, 89–106.
- Williams, C.J., Yamashita, Y., Wilson, H.F., Jaffé, R., Xenopoulos, M.A., 2010. Unraveling the role of land use and microbial activity in shaping dissolved organic matter characteristics in stream ecosystems. *Limnol. Oceanogr.* 55, 1159.
- Williamson, C.E., Stemberger, R.S., Morris, D.P., Frost, T.M., Paulsen, S.G., 1996. Ultraviolet radiation in North American lakes: attenuation estimates from DOC measurements and implications for plankton communities. *Limnol. Oceanogr.* 41, 1024–1034.
- Williamson, C.E., Morris, D.P., Pace, M.L., Olson, O.G., 1999. Dissolved organic carbon and nutrients as regulators of lake ecosystems: resurrection of a more integrated paradigm. *Limnol. Oceanogr.* 44, 795–803.
- Yallop, A., Clutterbuck, B., 2009. Land management as a factor controlling dissolved organic carbon release from upland peat soils 1: spatial variation in DOC productivity. *Sci. Total Environ.* 407, 3803–3813.
- Yu, Q., Tian, Y.Q., Chen, R.F., Liu, A., Gardner, G.B., Zhu, W., 2010. Functional linear analysis of in situ hyperspectral data for assessing CDOM in rivers. *Photogramm. Eng. Remote Sens.* 76, 1147–1158.
- Zhu, W., Yu, Q., 2013. Inversion of chromophoric dissolved organic matter from EO-1 hyperion imagery for turbid estuarine and coastal waters. *IEEE Trans. Geosci. Remote Sens.* 51, 3286–3298.
- Zhu, W., Yu, Q., Tian, Y.Q., Chen, R.F., Gardner, G.B., 2011. Estimation of chromophoric dissolved organic matter in the Mississippi and Atchafalaya river plume regions using above-surface hyperspectral remote sensing. *J. Geophys. Res. Oceans* 116.
- Zhu, W., Tian, Y.Q., Yu, Q., Becker, B.L., 2013a. Using Hyperion imagery to monitor the spatial and temporal distribution of colored dissolved organic matter in estuarine and coastal regions. *Remote Sens. Environ.* 134, 342–354.
- Zhu, W., Yu, Q., Tian, Y.Q., 2013b. Uncertainty analysis of remote sensing of colored dissolved organic matter: evaluations and comparisons for three rivers in North America. *ISPRS J. Photogramm. Remote Sens.* 84, 12–22.
- Zhu, W., Yu, Q., Tian, Y.Q., Becker, B.L., Zheng, T., Carrick, H.J., 2014. An assessment of remote sensing algorithms for colored dissolved organic matter in complex freshwater environments. *Remote Sens. Environ.* 140, 766–778.